A novel coating with universal adhesion and inflammation-responsive drug release functions to manipulate the osteoimmunomodulation of implants†

Min He, ‡[abc] Bo Yang,‡[abc] Fangjun Huo,[abc] Li Xie,[abc] Mo Yang*[d] and Weidong Tian*[abc]

Abstract

The immune response elicited by the bone endoprosthesis is currently considered an important factor that affects its interfacial osteointegration. In this work, a metal-phenolic-based drug-loaded coating with universal adhesion properties and intelligent drug delivery feature was created to promote osteointegration by manipulating a beneficial osteoimmune microenvironment. A novel pro-drug with inflammation-responsive release function was firstly synthesized via the esterification reaction between tannic acid (TA) and indometacin (IND), and then the coating was developed by chelating it with Fe3+. In the normal biological environment, the coating was stable, while, in the inflammatory environment, the release of TA and IND motifs could be triggered by the overexpressed esterase. The released TA and IND displayed synergistic effects on macrophage polarization, leading to a downregulation expression of pro-inflammatory cytokines, and an upregulation expression of anti-inflammatory cytokines and osteogenic-related factors. When stimulated by a conditioned medium generated by macrophages seeded onto the coating, the osteogenic differentiation potential of BMSCs was significantly enhanced. Finally, the designed coating significantly promoted the osteointegration of the implant, demonstrated by the increase of the bone-implant contact by two times. Additionally, the coating was substrate-independent and can be formed within seconds without special equipment, thus, it showed great potential applications to endow advanced hard tissue implants with favorable osteoimmunomodulation.

1. Introduction

A bone endoprosthesis, such as a dental implant, has been well developed and widely adopted to replace or restore the functions of damaged hard tissues. Despite achieving favorable clinical results, prosthesis loosening caused by insufficient osteointegration still remains one of the major reasons that is leading to implant failures. To address this issue, traditional strategies just directly targeted osteoblastic lineage cells by optimizing the physicochemical properties of bone biomaterials, usually resulting in inconsistencies between the in vitro and in vivo outcomes. Recently, the progress made in bone biology revealed the close relationship between immune and skeletal systems, cytokines secreted by immune cells is currently considered to be important regulators to mediate the balance of osteogenesis and osteoclastogenesis.1,2 Based on this principle, instead of the traditional one that just focused on osteoblastic cells,3,4 more attention on the design of next-generation advanced bone biomaterials should be paid on immunomodulatory properties, to manipulate a favorable osteoimmune environment so as to induce a beneficial balance of osteogenesis over osteoclastogenesis.

To develop such bone biomaterials, the dominant immune cells that participate in the bone regeneration process must be firstly clarified. Macrophages play a critical role in the implant-induced host immune response.5 After implantation, monocytes, anterior osteoblast cells, are rapidly recruited to the defect site and differentiate into macrophages, which are plastic and dynamic, may polarize toward two types in response to different signals: pro-inflammatory M1 phenotype or anti-inflammatory M2 phenotype.6,7 Sequential activation of macrophages toward M1 or M2 phenotype is essential for the normal bone tissue regeneration process. Generally, in the initial phase, macrophages mainly polarize towards the M1 phenotype and secrete pro-inflammatory cytokines, such as IL-1β, IL-6, and TNF-α, which have a significant influence on the bone marrow stem cell (BMSC)'s recruitment and subsequent differentiation.8 In the middle or later stage, macrophages mainly polarize to M2 phenotype, secreting anti-inflammatory cytokines (e.g. IL-4, IL-10) and osteogenesis-enhancing cytokines (e.g. BMP2, VEGF, and TGF-β1), to provide an anti-inflammatory microenvironment and promote new bone formation.9,10 However, being a foreign body, the implantation of bone biomaterials may elicit an unfavorable acute or severe immune response, inducing the persistence of pro-inflammatory M1 phenotype and being failure to timely switch to anti-inflammatory M2 phenotype, resulting in dentrimental osteoimmune environment.11 In detail, persisting M1 macrophages would upregulate expressions of those pro-inflammatory cytokines, a higher concentration of which would result in bone resorption.12 Therefore, the osteoimmunomodulation of hard tissue implants should be specially designed to enhance osteointegration. Currently, a moderate level of the inflammatory response induced by the implant is considered beneficial for osteointegration.

Recently, constructing a drug-loaded coating on implants has been demonstrated to be an effective strategy to manipulate a beneficial osteoimmune microenvironment.13–16 In those works, a hydrophilic hydrogel coating was firstly coated onto the implant surface, into which the immunomodulatory agent was then incorporated.17,18 The uncontrollable drug release, especially for the initial burst release, was still a great concern for these systems, for the reason that the uncontrollable release may lead to improper timing of M1 or M2 macrophage activation, resulting in dysfunctional healing in the form of chronic inflammation or fibrous encapsulation.19–21 In our previous work, a heparin-mimicking hydrogel thin layer was coated onto a substrate, and indometacin was conjugated via ester groups to obtain inflammation-responsive drug release.22 However, the fabrication procedures were complicated, needing multi-steps. In this study, a metal-phenolic-based drug-loaded coating with universal adhesion properties and inflammation-responsive release feature was constructed on Ti implants to promote osteointegration by manipulating beneficial osteoimmune microenvironment. A novel pro-drug was firstly synthesized via an esterification reaction between the selected phenolic ligand (tannic acid, TA) and indometacin (IND). As the most famous phenolic ligand, TA possesses many unique merits, including universal adhesion, chelating with metal ions, and antioxidant property.23–25 After grafting the IND molecule, the coating potential of TA–IND pro-drug could still be remained by precisely controlling the grafting ratio. This strategy presented the following advantages: it was a

simple, rapid, and universal strategy. With the assistance of Fe3+, the TA–IND coating could be easily deposited onto the substrate within seconds just by mixing the TA–IND solution and Fe3+ solution in the presence of the substrate. Due to the universal adhesion properties of metal/phenolic based coating, this coating strategy is substrate-independent, can be applied to almost any substrate regardless of its chemical composition, such as metal substrate, organic substrate, or inorganic substrate.26,27 The loaded drug molecule could be released in a smart manner. IND molecules were incorporated into the coating via inflammation-sensitive ester groups. In the normal biological environment, the coating was relatively stable, without obvious drug release, whilst, in the inflammatory milieu, the pro-inflammatory M1 macrophages would overexpress esterase, which was able to trigger the IND release by catalyzing the hydrolysis of ester groups.22,28–30 Therefore, the designed coating holds great potential to exhibit an on-demand, self-regulated, and feedback drug release profile, and the potential influence of the inflammation-responsive drug release profile on osteoimmunomodulation has not been well explored before. Additionally, the immunomodulatory function of TA has recently been focused on, which can regulate the immune response via the redox dependent signaling pathway.25,32 Along with the disassembling of the coating in the inflammatory environment, both TA and IND motifs could be released to synergistically manipulate the local osteoimmune microenvironment. We would systematically investigate the influence of the bio-responsive release behavior on the immune response, and the influence of the generated immune microenvironment on the final osteointegration.

2. Experimental methods

2.1 Materials

Tannic acid, indomethacin, *N*,*N*′-dicyclohexylcarbodiimide (DCC), 4-dimethylaminopyridine (DMAP), iron chloride, 1, 1-diphenyl-2-picrylhydrazyl, and tetrahydrofuran (THF) were purchased from Aladdin Chemistry Co. Ltd and used as received. Polycaprolactone (PCL), 2,2-diphenyl-1-picrylhydrazyl (DPPH), and 2-phenly-4,4,5,5-tetramethylimidazoline-3-oxide-1-oxyl (PTIO) were purchased from Sigma Aldrich Co. Ltd. Pure Ti plates (Grade 1) with a diameter of 15 mm and a thickness of 1 mm were purchased from Suzhou Chuanmao Metal Materials Co. Ltd, and used as the model substrate. Dulbecco's modified Eagle medium, fetal bovine serum, 0.05% Trypsin EDTA, CCK-8 agent, and phosphate-buffered saline (PBS, pH 7.4) were purchased from Gibico Co. Ltd.

2.2 Specimen preparation

Synthesis of TA–IND

TA–IND was synthesized *via* the esterification reaction in THF with the presence of DCC and DMAP. In a typical reaction, IND (5.0 g, 14 mmol) and TA (23.8 g, 14 mmol) were dissolved in

dry THF (180 mL), DCC (5.8 g, 28 mmol) and DMAP (0.25 g, 2 mmol) were dissolved in another 20 mL dry THF. Then, the mixture containing DCC and DMAP were added dropwise in the solution containing TA and IND over a period of 10 min with continuous stirring. The reaction mixture was stirred at 0 °C for 1 h and then at room temperature for 24 h. After that, the reaction solution was filtered to remove the impurities before precipitation into cold water to obtain a light-yellow powder product, which was dried at room temperature under vacuum. By controlling the mole ratio of TA and IND, various TA–INDs with different IND grafting degree could be obtained, for example, TA-3IND and TA-5IND were synthesized following the same procedures.

Formation of TA–IND coating

Pure Ti sheets (99.6% purity) with a diameter of 1.2 cm were selected as the model substrate. The cleaned Ti plates were immersed in 10 mL of 6 mg mL^{-1} TA–IND solution in THF for 3 min, then 10 mL 18 mg mL^{-1} $FeCl_3$ solution in water was added dropwise with mildl shocking. Then, the pH value of the mixture was adjusted to 8.0 by adding 0.5 mol L^{-1} NaOH dropwise. Then, the plates were rinsed with deionized water. To increase the thickness of the coating, this deposition process was repeated 5 times.

2.3 Physicochemical property characterizations of the TA–IND coatings

The surface roughness and morphology were observed using atomic force microscopy (AFM, SPI 3800, NSK Inc., Japan) and field emission scanning electron microscopy (SEM, JSM-6390, JEOL, Japan). The chemical compositions were studied using X-ray photoelectron spectroscopy (XPS, K-Alpha, Thermo Electron). The coating thickness was evaluated by a spectroscopic ellipsometer with a Cauchy model to finalize the determination. The measurement of electron paramagnetic resonance (EPR) was carried out to analyze the chelation of Fe^{3+} to TA–IND. The surface wettability of the coatings was evaluated by measuring the water contact angles with a contact angle instrument (Powereach jc2000D1Zhong-Cheng Digital, China).

2.4 *In vitro* drug release study

The IND-loading amounts in these coatings were evaluated by completely digesting the coatings with 1.5 mL of 50 U mL^{-1} esterase solution in PBS. After 12 h treatment at 37 °C, the OD values of the digestion solutions at 320 nm were measured using an ultraviolet-visible spectrophotometer, and IND contents were calculated according to the standard curve of IND. To investigate the inflammation-responsive IND release behavior, TA-5IND coating was selected as the model and incubated at 37 °C in 2 mL PBS with various esterase concentrations, and IND release amounts were determined using an ultraviolet-visible spectrophotometer (UV2550, Shimadzu, Japan). To further investigate the interactions between coatings and macrophages, 1×10^5 RAW264.7 cells were seeded onto Ti-5IND coatings. After 12 h, the culture medium of one group was replaced by the normal culture medium, while another group's medium was replaced by the medium containing 2 mg mL^{-1} LPS. After a further 24 h co-

culturing, the supernatants were collected and centrifuged before analysing them on an ultraviolet-visible spectrophotometer.

2.5 Radical scavenging assay

The 2,2-diphenyl-1-picrylhydrazyl (DPPH) method, 2-phenly-4,4,5,5-tetramethylimidazoline-3-oxide-1-oxyl (PTIO) method, and hydroxyl-free radical scavenging capacity assay kit was used to evaluate the radical scavenging properties of TA-0IND, TA-1IND, TA-3IND, and TA-5IND coatings. For the DPPH method, each sample was added to a 24-well plate, and then 1 mL DPPH/ethanol (10.3 μmol mL^{-1}) was added to each well. Subsequently, the plates were incubated at 37 °C for 1 h, then the absorbance of the supernatant was read using an ultraviolet-visible spectrophotometer at 570 nm. For the PTIO method, each sample was fixed into a 24-well plate, and then 0.5 mL PTIO water solution (0.6 μmol mL^{-1}) was added in each well and incubated at 37 °C for 4 h. Then, the absorbance of the supernatant was read at 557 nm. The hydroxyl-free radical scavenging capacity evaluation was carried out according to the manufacturer's instructions.

To further evaluate the intracellular ROS scavenging capacity of coatings, 5×10^4 RAW264.7 cells were seeded on the coating surfaces. After 12 h, the cells were further stimulated by 2.0 μg mL^{-1} LPS for another 6 h culturing. The DCFH-DA and DAPI probes were added and incubated for 30 min before imaging with confocal laser scanning microscopy (CLSM).

2.6 *In vitro* biocompatibility evaluation

Raw264.7 macrophage cells and rBMSCs were used to evaluate the *in vitro* biocompatibility of the coating. 1×10^4cells were seeded on each sample. The cells' proliferation at 1, 3, and 5 days were detected by CCK-8 assay (KeyGEN BioTECH, Nanjing, China). The cells' morphology on the coatings was observed by SEM and CLSM. The detailed procedures are provided in the ESI† (S2.6).

2.7 Immunomodulatory property evaluation of the coatings

Gene expression of macrophages on the coatings

1.5×10^5 cells were seeded onto the coatings. After culturing for 4 days, the total RNA from the cells was extracted and were used to synthesize complementary DNA. Then, RT-PCR assay was applied to detect the expression of inflammatory genes (IL-1β, IL-6, TNF-α, IL-4, IL-10), macrophage phenotype markers (CD86 for M1, CD-206 and CD163 for M2), osteogenic-related genes (BMP-2, TGF-β1, VEGF), and osteoclastic-related genes (TRAP and CTSK). Detailed procedures are provided in the ESI† (S2.7), and information on RNA primers used in this work is provided in the ESI† (Table S1).

Cytokines expressions of macrophages on the coatings

To systematically investigate the *in vitro*osteoimmune environment generated by macrophages culturing on the coatings, the concentration of some representative pro-inflammatory and anti-inflammatory cytokines was detected by ELISA kit. The detailed procedures are provided in the ESI.†

The *in vivo* immunomodulatory property evaluation of the coatings was conducted on the subcutaneous implantation model of mice. The animal experiments were approved by the Animal Care Committee of West China of Stomatology Sichuan University. For the convenience of fixing samples and tissue sections, in this section, the coatings were deposited onto PCL nanofibrous membrane. An incision was made on the middle of the back of the mouse, one sample (10 mm squares) was inserted, and the incision was closed gently. After 4 and 7 days, the mice were sacrificed, and the skin covering the implants was harvested and fixed in paraformaldehyde. The obtained tissue sections were used for H and E staining, immunohistochemical staining, and immunofluorescence staining. The staining procedures were carried out according to the previous work.

2.8 Osteoimmunomodulatory (OIM) property of the coatings

To investigate the OIM properties of the coatings, 5.0×10^4 macrophages were firstly seeded onto the coatings. After culturing for 4 days, the supernatants were collected and centrifuged. The conditioned medium was prepared by mixing the collected supernatants with the osteogenic induction medium in the volume ratio of 1 : 1. Then, 1.5×10^5BMSCs were cultured in each well of a 6-well plate for 12 h, then the medium was replaced by the collected conditioned medium for another 7 day culture. Total RNA was harvested, and RT-qPCR was performed to detect the expression levels of osteogenic-related genes (BMP2, COL1, OCN, VEGFA, ALP, and RUNx2) and osteoclastogenic-related genes (CTSK, TRAP, and MMP9). The details of the RNA primers used in this work are provided in the ESI†(Tabel S1).

To further confirm their osteogenic differentiation potential, 1.5×10^4 BMSCs were cultured in each well of a 24-well plate for 12 h, then the medium was replaced by the collected conditioned medium. After culturing for another 7 days or 14 days, ALP staining and alizarin Red staining were used to highlight ALP secretion and mineralization nodule formation potential, respectively, of BMSCs cultured in the conditioned medium. Detailed procedures are provided in the ESI† (S2.8).

To investigate the *in vivo* osteointegration efficiency of the coatings, the pristine Ti bar and coating-modified Ti bars were inserted parallel to the long axis in the femurs of mice for 8 weeks. When the mice were sacrificed, the femurs containing the implants were harvested and subjected to micro-CT scanning. To analyze the newly-formed bone tissues around the implants, the undecalcified sections were also acquired and used for H and E staining and toluidine blue staining.

2.9 Statistical analysis

All quantitative data are expressed as mean ± standard deviation. Statistical analyses were performed using the SPSS 19.0 software (Chicago, IL). Statistical differences were determined using Student's *t*-test for independent samples. Differences between groups of $*p < 0.05$ were considered statistically significant.

3. Results and discussion

3.1 Formation of TA–IND/Fe^{3+} coatings

To fabricate the IND-loaded intelligent coating, pro-drug (TA–IND) was firstly synthesized *via* the esterification reaction between the hydroxyl group of tannic acid (TA) and the carboxyl group of indometacin (IND). TA was selected as the phenolic ligand for its universal adhesion properties and sufficient phenolic hydroxyl groups as linking sites of IND molecules.[31] The chemical structure of TA–IND was characterized using FTIR and ^{13}C NMR (Fig. S1, ESI†). By comparing FTIR spectra of TA and TA–IND, it was clearly found that the characteristic peak of CH_3- from IND appeared at 2813 cm^{-1} for TA–IND samples. Both the characteristic peaks of TA and IND were found in the ^{13}C NMR spectrum of TA–IND, demonstrating that the TA–IND prodrug was successfully synthesized.

The formation of metal/phenolic coating is mainly dependant on the functions of universal adhesion property and chelation with metal ions of phenolic ligand.[32] Generally, after mixing TA and Fe^{3+} solutions in the presence of a substrate, a small fraction of free TA molecules would rapidly adhere onto the substrate surface due to its good adsorption ability rendered by its catechol moieties and the adhered TA molecules would simultaneously be crosslinked by Fe^{3+}, meanwhile, most TA molecules in the solution are cross-linked by Fe^{3+} to form TA/Fe^{3+}complexes, and some complexes would deposit onto the substrate and further cross-linked by the excess Fe^{3+} to form a rough coating.[33] The whole process is accomplished within seconds. After grafting IND onto TA molecules, the molecular conformation would be significantly changed, which may result in the loss of coating potential. In addition, due to sufficient phenolic hydroxyl groups, each TA molecule could link a different number of IND molecules. However, over-consumption of the phenolic hydroxyl groups may also impair the coating potential of TA–IND. By controlling the molar ratio of TA and IND in the esterification reaction system at 1 : 1, 1 : 3, and 1 : 5, we synthesized TA-1IND, TA-3IND, and TA-5IND, respectively. Then, the versatile coating capability of TA–IND was investigated by depositing TA-5IND coating onto the Ti plate, PCL nanofibrous membrane, and halloysite nanoparticles, and the obvious surface color changes verified that the TA-5IND molecule could still maintain its universal coating capability (Fig. 1(A)). The surface morphologies of these coatings on Ti plates were further investigated using SEM and AFM (Fig. 1(B) and (C)). The coatings were uniformly distributed on Ti plates and displayed a rough morphology, which looked like a monolayer assembly of spheroid agglomerates. The size of spheroid agglomerates increased with the increase of the IND grafting degree, leading to a rougher surface morphology, with the increase in Ra values from 2.44 nm to 13.61 nm. TA molecule is hydrophilic, while IND molecule is hydrophobic. So, the synthesized TA–IND is amphiphilic. According to the phenomenon that surface morphology changed with IND-grafting ratio, the formation mechanism of the coatings may be governed by the hydrophilic–hydrophobic interactions of amphiphilic TA–IND molecule, instead of metal/phenolic surface chemistry. To clarify the formation mechanism of the coating, the EPR spectra was further performed to analyze the products harvested from the reaction systems of TA–IND and Fe^{3+}, and significant signals of metal-phenolic networks were detected at around 10 G, verifying the contribution of metal-

phenolic chemistry to the formation of the coating (Fig. S2, ESI†). Therefore, the formation of the coating was synergistically governed by the hydrophilic–hydrophobic interactions of TA–IND molecules and the metal-phenolic chemistry between the TA–IND molecule and Fe^{3+}.

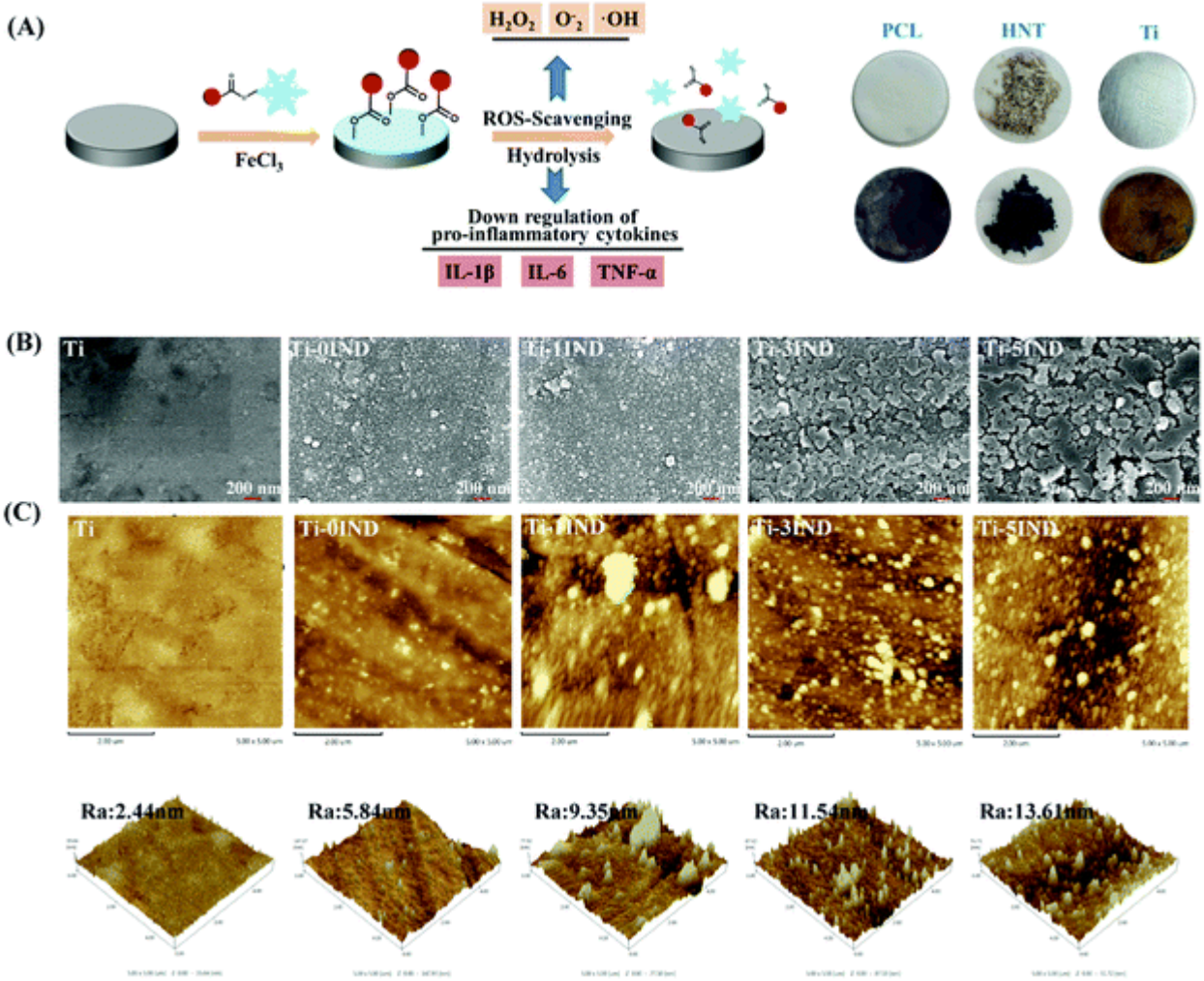

Fig. 1 (A) Illustration of the universal coating processes of TA–IND/Fe^{3+} coating and its immunomodulatory mechanism; (B and C) surface morphology of the coatings observed by SEM and AFM.

To analyze the surface chemical compositions of the coatings, energy-dispersive spectrometry (EDS) mapping was conducted, and the Cl element originating from the IND molecule was selected as a characteristic element. The characteristic signal of the Cl element (red dots) gradually intensified with the increase of the IND grafting degree, implying that the drug loading efficiency of the coatings could be adjusted by controlling the IND grafting degree (Fig. 2(A)). Before analysis by XPS, these coating-capped Ti plates were firstly immersed in $AgNO_3$ solution.[34] Compared with the pristine Ti plate (Fig. 2(C)), besides the emerged new peaks associated with Cl and N from IND, the emergence of the characteristic peak of Fe element further verified the contribution of metal-phenolic chemistry on the formation of the coatings. The emergence of Ag characteristic peaks suggested that the remaining TA motifs could render the membrane antioxidant potential, implying that the coatings were able to modulate the immune response not only depending on releasing IND but also through tuning of

the redox signaling pathway.[27] In addition, due to the inherent hydrophilicity of TA molecules, the wettability of coatings was also significantly affected by the remaining TA motifs. As shown in Fig. 2(B), the Ti plate showed a WCA of around 61°, while the Ti-0IND was superhydrophilic with a WCA of around 15°. Due to the hydrophobic property of IND, as the IND-grafting ratio increased from 0 to 5, WCAs of the corresponding coatings increased from 17° to 85°. The surface wettability changes implied that the coatings possessed the potential ability to affect protein adsorption, cell adhesion, even macrophage polarization.[35]

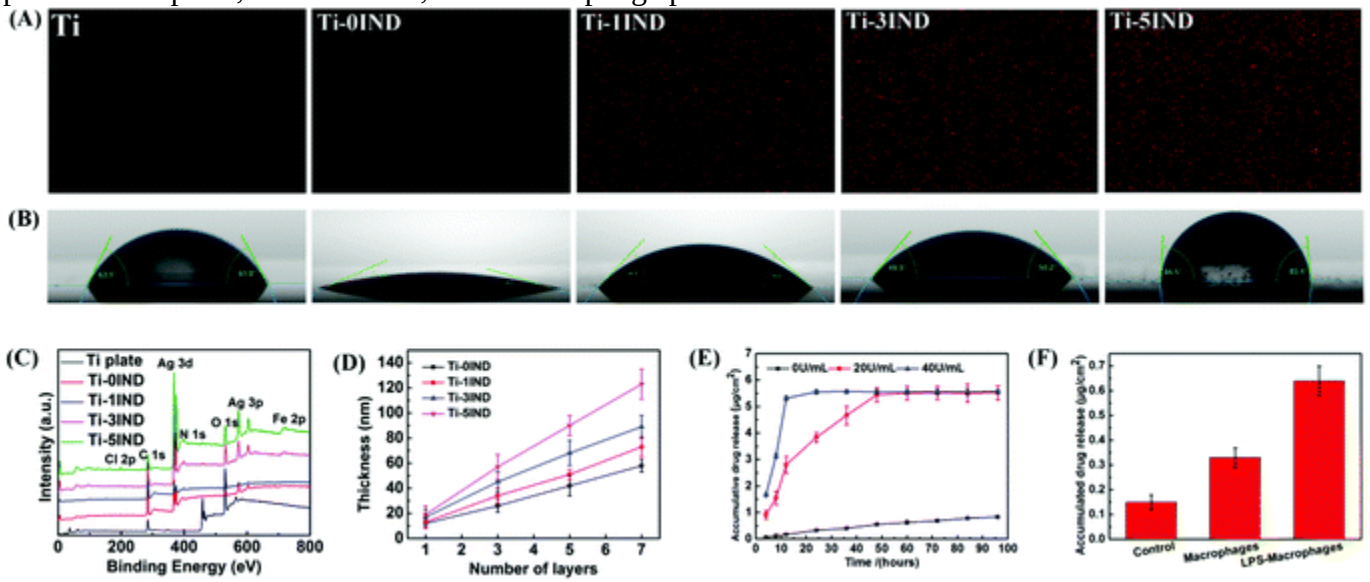

Fig. 2 (A) EDS mapping of the coatings with Cl as the characteristic element; (B) images of water contact angle (WCA); (C) XPS spectra of the coatings after immersing in $AgNO_3$ solution; (D) the relationship between the repeating times and the coating thickness. (E) IND release profiles triggered by esterase with different concentrations. (F) IND release amounts from TA-5IND coating immersed in cell culture medium, macrophage supernatant, and LPS stimulated macrophage supernatant, respectively.

3.2 Drug release profile of the coating

As mentioned above, the drug loading amounts of the coatings could be adjusted by controlling the IND-grafting ratio. Another manner to increase the drug loading efficiency is to increase the coating thickness. According to the formation mechanism of the metal-phenolic-based coating, the feed concentration of Fe^{3+} and TA–IND, and the size of the TA–IND/Fe^{3+} complex aggregates rather than the coating time, would finally determine the coating thickness. By keeping a constant feed concentration of TA, TA-1IND, TA-3IND, and TA-5IND at 2.4 mM and Fe^{3+} at 7.2 mM, uniform coatings with thicknesses of 12 ± 3 nm, 16 ± 5 nm, 18 ± 6 nm, and 19 ± 5 nm were formed, respectively, on Ti plates within seconds. Changing the feed concentration of Fe^{3+} and TA–IND would not lead to a significant influence on the coating thickness, and the obtained drug-loading efficiency may be insufficient to modulate the immune response. However, the coating thickness could be further increased by repeating the coating process. As shown in Fig. 2(D), the coating thickness displayed a linear relationship with the repeating times. In this work, the coating process was repeated five times, and final coating thicknesses of 42 ±

8.7 nm, 51 ± 4.5 nm, 68 ± 9.2 nm, and 92 ± 8.3 nm were obtained for Ti-0IND, Ti-1IND, Ti-3IND, and Ti-5IND, respectively.

The quantitative analysis of IND contents was carried out by completely digesting the coating with cholesterol esterase (CE), then the OD values of the digestion solution at 320 nm were read using an ultraviolet-visible spectrophotometer, and IND content was calculated according to the standard curve of IND. As a result, the IND loading amounts were 0.7 ± 0.1 μg cm^{-2}, 2.6 ± 0.3 μg cm^{-2}, and 5.6 ± 0.4 μg cm^{-2} for Ti-1IND, Ti-3IND, and Ti-5IND, respectively. CE solution in PBS was used to mimic the inflammation environment to further investigate the IND release profile. As shown in Fig. 2(E), IND molecules could be slowly released from the coating due to the spontaneous hydrolysis of ester groups, while the release rate could be significantly accelerated by CE and displayed a dose-dependent relationship. As mentioned above, macrophages would overexpress esterase in the inflammation environment caused by the implant,[36] so mouse macrophages were seeded onto Ti-5IND and cultured with or without LPS for 24 h to confirm the inflammation-responsive release behavior of IND. Compared with the control sample (without macrophages), the enzymes secreted by macrophages were capable of inducing IND release from the coating, and the LPS stimulated macrophages enhanced enzyme accumulation, leading to faster IND release (Fig. 2(F)). It was noteworthy that the hydrolysis of ester groups in the coatings did not only lead to the release of IND molecules but also the release of pyrogallol and catechol groups of TA, which also played a vital role in the immunomodulation function of the coatings.

3.3 ROS scavenging ability evaluation

Although low levels of ROS are essential for regulating oxygen homeostasis and cellular signaling, continuous high levels of ROS caused by the implant-related inflammatory response can induce oxidative stress that would damage surrounding normal tissue.[37,38] Above analysis confirmed that the residual phenolic hydroxyl groups could still render the coating antioxidation property. Thus, the radical scavenging property of these coatings was evaluated using the DPPH method, PITO method, and a commercially available kit of hydroxyl radical elimination. As shown in Fig. 3(A), the three radical scavenging evaluation models showed similar results that the radical scavenging ability was well preserved in all coatings, but decreased with the increase in the IND-grafting ratio caused by the decrease of the surface phenolic hydroxyl density. To further assess the ROS elimination capacity, macrophages were seeded onto the coating surface and activated to pro-inflammatory M1 phenotype by lipopolysaccharide (LPS).[39] The intracellular ROS levels were detected by DCFH-DA (green fluorescence) kit. As shown in Fig. 3(D), the LPS treated RAW264.7 cells seeded on pristine Ti showed a strong green fluorescence, while a dramatic decrease in the green emission was observed on the coatings, and displayed a tendency of decrease with the increase of the IND grafting degree. This result should be ascribed to the interactions between macrophages and the coatings. As analyzed above, in the inflammation environment, the overexpressed esterase would lead to hydrolysis of ester groups, resulting in the release of IND, pyrogallol, and catechol moieties. In turn, pyrogallol and catechol groups were able to scavenge the generated ROS, while the IND molecules would inhibit the generation of ROS by suppressing the inflammation response. ROS plays a critical role in inflammation processes, so TA and IND motifs have great potential to show a synergistic effect on the local immune environment.

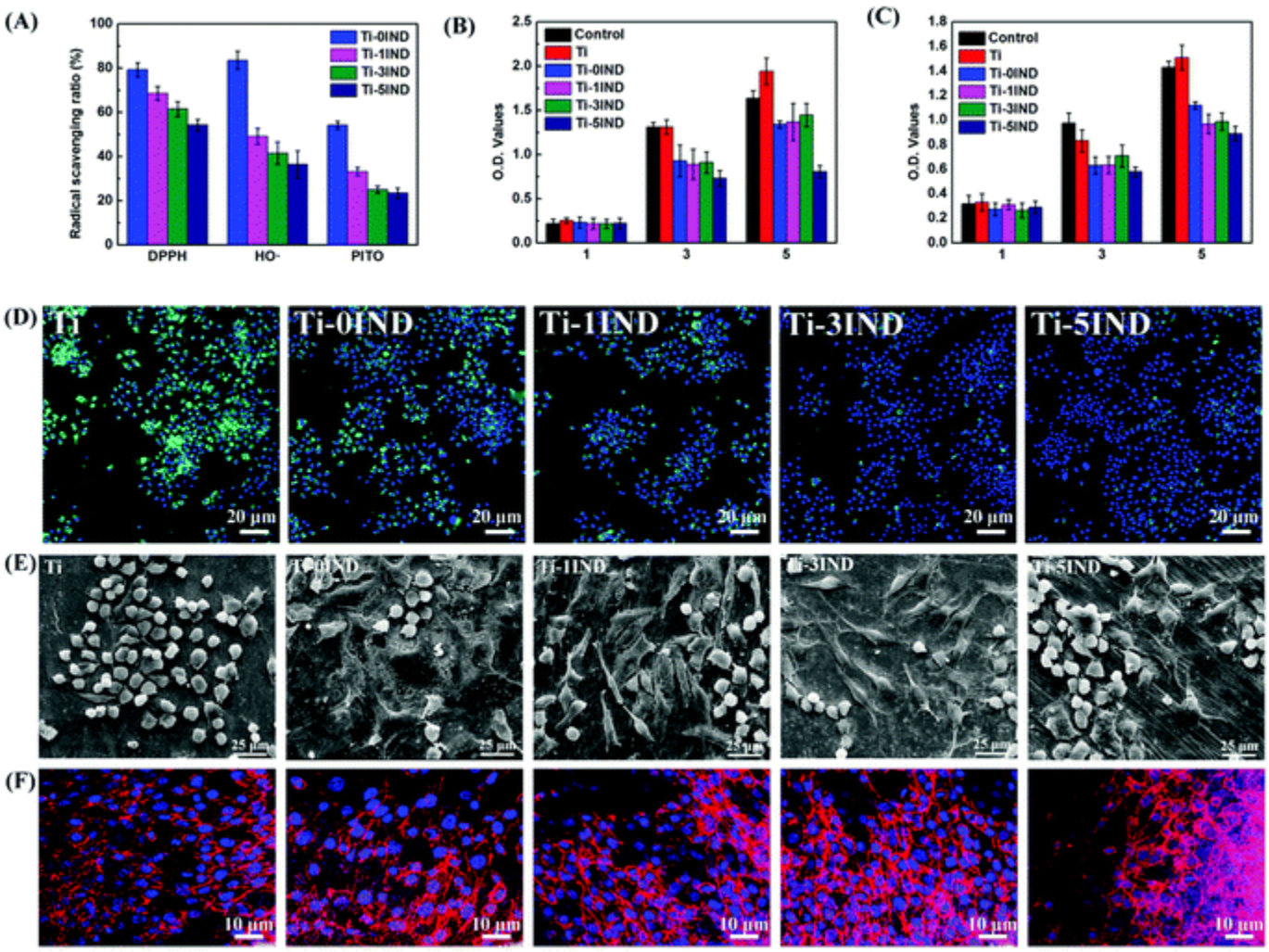

Fig. 3 (A) ROS-eliminating capability of the coatings: elimination of DPPH; elimination of hydroxyl radical; elimination of PITO; Proliferation of RAW264.7 cells (B) and BMSCs (C) on the coatings detected by CCK-8 assay; (D) the intracellular ROS generation of RAW264.7 cells seeded on the coatings; (E) the RAW264.7 cells' morphologies on the coatings for 5 days observed by SEM; (F) the BMSCs's morphologies on the coatings for 5 days observed by confocal microscopy.

3.4 *In vitro* biocompatibility evaluation

For the *in vitro* biocompatibility evaluation, both RAW264.7 cells and BMSCs were seeded on the coatings. The CCK-8 assay was carried out to evaluate the proliferation of these cells, and the results indicated that all coatings could continuously support cells' proliferation (Fig. 3(B) and (C)). However, compared with TCP and the Ti plate, the cell viability on these coatings was obviously inhibited. The possible reason may be ascribed to the residual phenolic hydroxyl groups of TA, which displayed high reactivity toward amine groups of cell membrane proteins,[24] and the released IND molecules, which inherently possessed an inhibition effect on macrophage viability.

The morphology of macrophages on different surfaces was observed by SEM (Fig. 3(E)). Compared with the pristine Ti plate, macrophages seemed to attach, extend, and integrate better on the coatings, having larger cell attachment areas and more extended pseudopodia, indicating better cell affinity. The results may be ascribed to the improved surface wettability of the coatings; it has been reported that surface wettability affects cell adhesion and spreading by affecting nonspecific protein adhesion.[40] Additionally, most macrophages displayed a round shape on pristine Ti plate, while the cells seemed to spread flatter and showed more diversity on Ti-0IND coating. For Ti-1IND, Ti-3IND, and Ti-5IND coatings, more cells displayed spindle-like cell morphology. Macrophage morphology is generally associated with their polarization state.[41,42] Therefore, the striking difference in macrophage morphology on different coatings is an effective indicator that implies a potential immunomodulatory function of the coatings.

Additionally, angiogenesis at the bone-implant interface is recognized as a prerequisite for osteointegration.[43]Some reports revealed that immunomodulators could inhibit the angiogenesis process. So, the angiogenic activity of the HUVECs on the coatings was investigated by evaluating the proliferation and vascularization capacity of HUVECs. The results indicated that HUVECs displayed a similar proliferation profile and viability to RAW264.7 and BMSCs (Fig. S3. ESI†). To further evaluate their angiogenic ability, HUVECs were incubated on matrix gel in the conditioned medium generated by macrophages seeded on the coatings, and the number of capillary-like structures in the gel was analyzed according to the photographs taken at 3 and 7 hours. The results also did not display a significant difference between the coatings and the control group (Fig. S4, ESI†).

3.5 Immunomodulatory function of the coatings

As mentioned above, macrophages play the most important role in manipulating the osteoimmune microenvironment. After implantation, macrophages are rapidly recruited to the implantation site and sequentially polarize to its M1 and M2 phenotypes to participate in regulating the osseointegration process. In this study, macrophages were cultured on the coating surfaces for 4 days to investigate the effects of the coatings on macrophage biological behaviors by determining the fold changes of some representative genes related to macrophage's surface markers, pro-inflammation, anti-inflammation, osteogenic, and osteoclastic by RT-PCR. We firstly defined the phenotype of macrophages on different coating surfaces by investigating the expression of their surface marker genes (M1: CD86, M2: CD206 and CD163) (Fig. 4(A)). Compared with the control group (macrophages were directly cultured on the culturing plate), the expression of the M1 marker was enhanced for the pristine Ti plate group, and was inhibited for all coating groups, whilst, the expression of M2 phenotype markers was significantly upregulated for the IND-loaded coatings. It is noteworthy that the coating without IND loading (Ti-0IND) did not significantly affect the expression of the M2 phenotype surface markers. The results implied that the TA coating could inhibit the polarization of macrophages toward the M1 phenotype, while the TA–IND coatings could inhibit macrophages' polarization towards the M1 phenotype and simultaneously promote its M2 phenotype polarization.

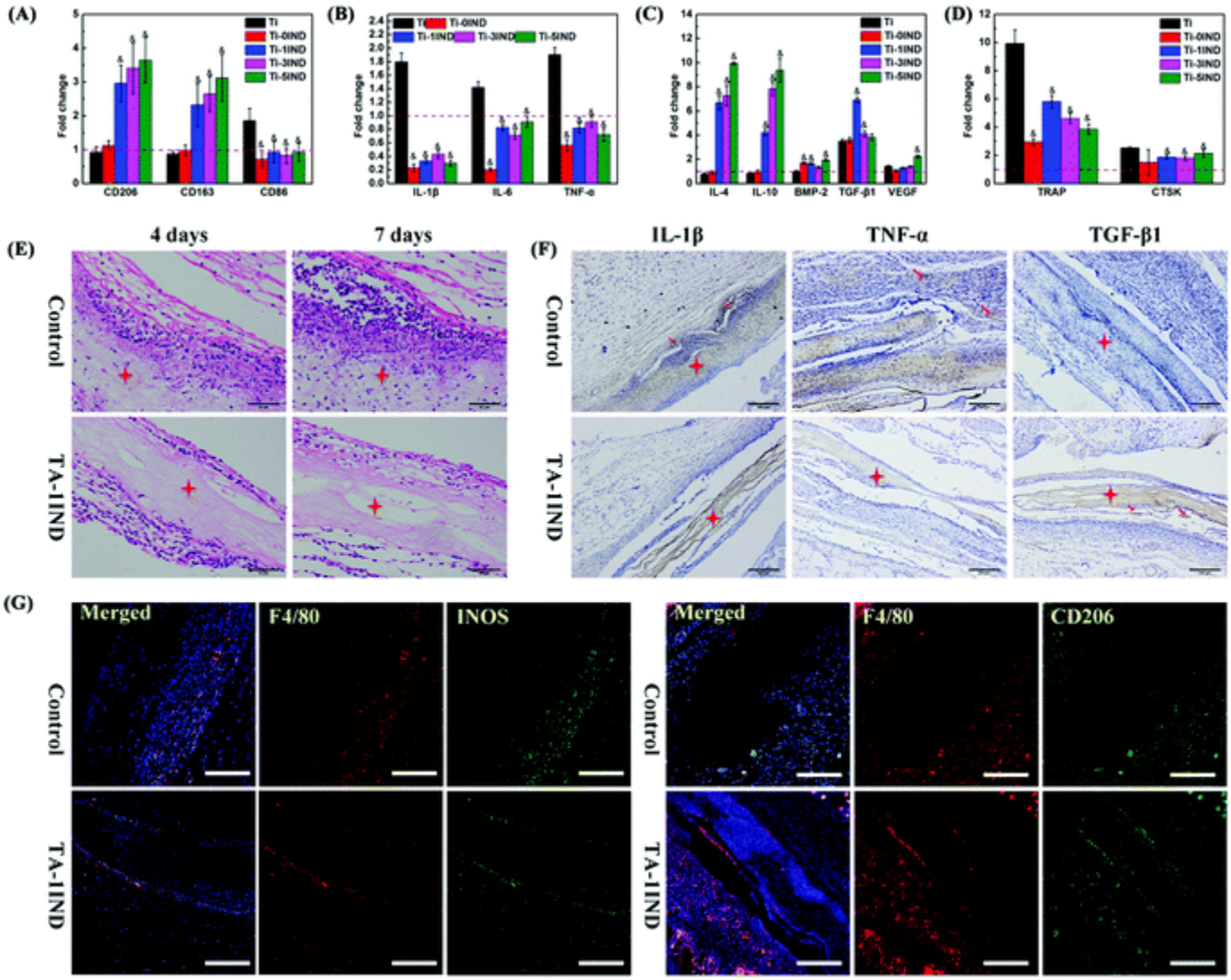

Fig. 4 Effects of the coatings on macrophages gene expression: (A) surface marker genes (M1: CD86; M2: CD206 and CD163); (B) pro-inflammatory genes (IL-1β, IL-6 and TNF-α); (C) anti-inflammatory genes (IL-4, IL-10, BMP-2, TGF-β, and VEGF); (D) osteoclastogenic-related genes (TRAP and CTSK). [&]Significant difference ($P < 0.05$) compared to the Ti plate group. (E) images of H&E staining, immunohistochemical staining, and immunofluorescence staining of the obtained subcutaneous tissues.

Correspondence with the results of macrophage polarization on these surfaces, macrophages on the Ti plate surface mainly expressed the pro-inflammatory related genes (IL-1β, IL-6, TNF-α). The downregulation of the inflammatory-related genes was more pronounced in cells cultured on TA coating compared with TA–IND coatings. The expression of anti-inflammatory related genes (IL-4, IL-10) was significantly upregulated on the TA–IND coatings, and the upregulation extent increased with the increase of the IND grafting degree (Fig. 4(B) and (C)). Besides inflammatory-related factors, macrophages can also release BMP2, TGF-β1, and VEGF factors to regulate osteogenesis, fibrosis, and angiogenesis.[5] So, the expression of BMP2, TGF-β1, and VEGF was also assessed to fully define the osteoimmune environment. As shown in Fig. 4(C),

compared with TCP and the Ti plate, all the coatings upregulated the expression of BMP2. All surfaces, especially for Ti-1IND, significantly enhanced the expression of TGF-β1. For VEGF expression, upregulation extent increased with the increase of IND grafting degree. In an abnormal immune microenvironment, macrophages would differentiate into osteoclast, leading to an imbalance between osteogenesis and osteoclastogenesis, resulting in bone resorption.[44] Osteoclasts break down bone tissue by secreting proteases, and TRAP and CTSK are the two main proteases involved in degrading type I collagen, so the expressions of TRAP and CTSK for macrophages on these surfaces were investigated. All the coatings significantly suppressed the expression of TRAP and CTSK (Fig. 4(D)).

Implants tended to induce mild or moderate inflammatory responses to trauma during implant surgery. To investigate the immunomodulation function of the coatings in an inflammatory environment, LPS was used to activate the macrophages seeded onto the coatings to mimic the *in vitro* inflammatory response. The concentration of representative cytokines secreted by M1 and M2 macrophages, such as IL-1β, IL-6, TNF-α, and IL-10, was determined by ELISA. All the coatings inhibited the secretion of the pro-inflammatory cytokines, and TA coating displayed a more significant inhibitory effect than TA–IND coatings. However, almost no anti-inflammatory cytokine secretion was detected on the TA coating, which was enhanced on the TA–IND coatings (Fig. S5, ESI†). The results of ELISA were highly consistent with those of PCR assay.

Then, *in vivo* immunomodulatory function of these coatings was evaluated by the mice subcutaneous implantation model. The movement of the hard Ti plate makes it difficult to obtain the subcutaneous tissue that contacts with the coating, and special equipment are necessary to obtain hard tissue slice. For the convenience of the experiment, in this section, PCL fibrous membrane was used as the model substrate.

The above analysis indicated that a higher IND grafting ratio could slightly decrease the cell viability, and Ti-0IND coating could only inhibit the macrophages' polarization toward the M1 phenotype. Therefore, TA-1IND coating was selected as the representative for the further *in vivo* investigation, and pure PCL membrane was used as a control. To evaluate the inflammatory level and different phenotypes of the macrophages recruited to the surrounding of the implants, we conducted H and E staining, immunohistochemical staining, and immunofluorescence staining on the obtained tissue sections. A larger number of inflammatory cells were infiltrated around or into the pure fibrous membrane, while less inflammatory cells were observed around the coating modified membrane and no cells infiltration into the membrane was observed. The thickness of the fibrous layer for the coating-modified membrane was thinner than that of the pure membrane, indicating that a milder inflammatory response was induced by the modified membrane (Fig. 4(E)). Immunohistochemical staining of the fibrous layer indicated that inflammatory cells gathered around pure PCL membrane secreted more pro-inflammatory cytokines and less anti-inflammatory cytokine than cells around the modified membrane (Fig. 4(F)). The results of immunofluorescence staining further demonstrated that a higher proportion of M2 phenotype macrophages was dominated around the coating-modified membrane, whereas more M1 phenotype macrophage were around the pure membrane (Fig. 4(G)). Therefore, the *in vivo* results had a good consistency with that of *in vitro* evaluation and collectively demonstrated that the TA–IND coating can promote macrophage polarization toward the M2 phenotype and manipulate an anti-inflammatory environment.

3.6 Osteoimmunomodulatory potential evaluation

After understanding the immunomodulatory function of the coatings, the next step was to research the effects of the generated osteoimmune environment on osteogenic differentiation. The culture medium generated from macrophages cultured on the Ti plate or the coating surfaces was collected, where the conditioned medium (CM) was prepared by mixing the culture medium with the osteogenesis induction medium with the volume ratio of 1 : 1. Then, BMSCs were incubated with CM for 7 days, and their osteogenic differentiation ability was firstly studied by RT-PCR by determining the expression of osteogenic and osteoclastogenic related genes, *i.e.*, BMP2, COL-1, VEGF, ALP, OCN, RUNX2, CTSK, TRAP, and MMP9. Compared with the Ti plate, both Ti-0IND and Ti-1IND coatings enhanced the expression of the osteogenic genes, and downregulated the expression of osteoclastogenic genes, especially for Ti-1IND (Fig. 5(A) and (B)). ALP staining was also performed to evaluate the ALP expression in BMSCs that was cultured with CM for 7 days. As shown in Fig. 5(D), consistent with the results of gene expression, the ALP expression in the Ti-1IND group was higher than that of the Ti-0IND group, followed by the Ti group. After culturing in the conditioned medium for 14 days, Alizarin red staining was conducted to investigate the mineralization level of BMSCs in CM. More calcified nodules were stained red in the coating groups (Fig. 5(E)), and the trend was further confirmed by the quantitative test (Fig. 5(C)).

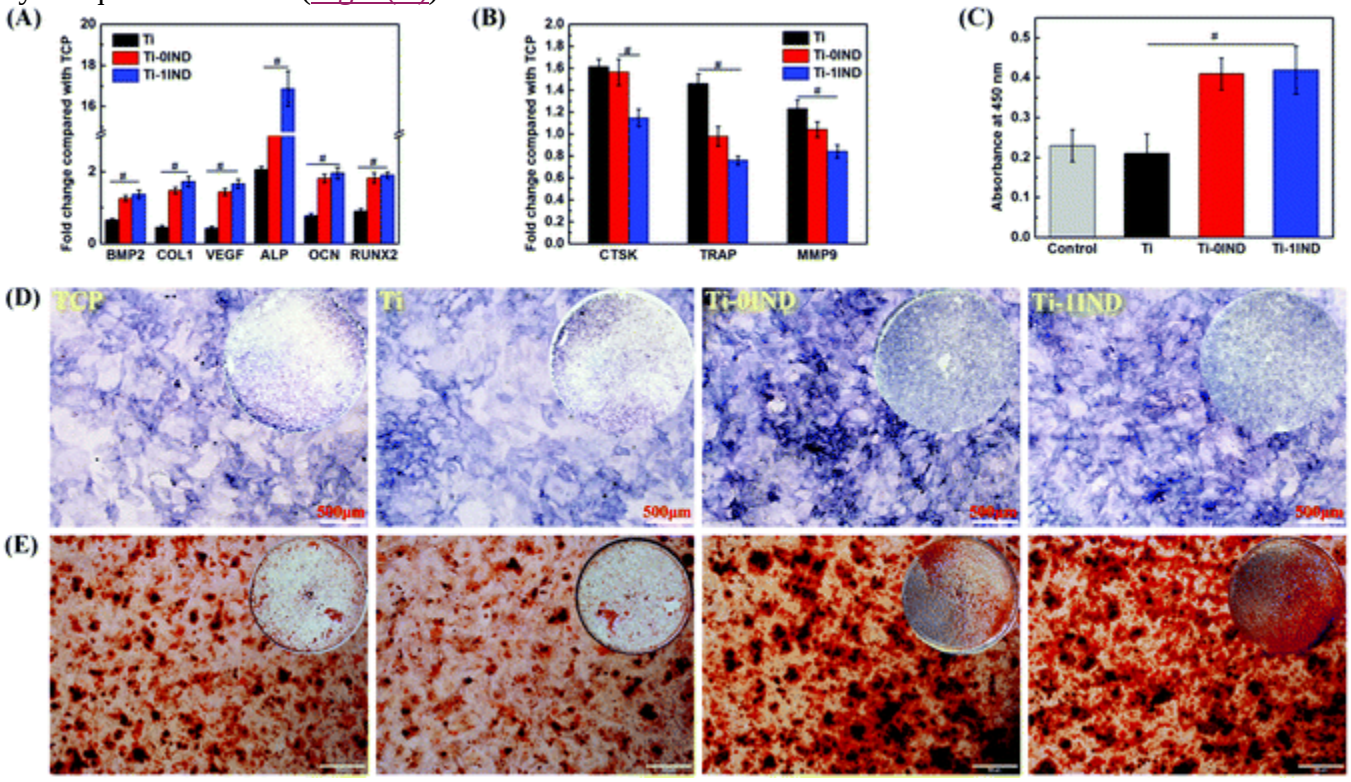

Fig. 5 Expressions of osteogenesis factors (A) and osteoclastogenic factors (B) detected by RT-qPCR; (C) quantitative analysis of alizarin red results; (D) images of ALP staining for BMSCs cultured in the conditioned medium for 7 days; (E) images of alizarin red staining for BMSCs cultured in the conditioned medium for 14 days. *Significant difference ($^{\#}P < 0.05$) compared with the Ti plate.

The *in vitro* results made us to further investigate the *in vivo* osteointegration efficiency of the coating-modified Ti bar. The pristine Ti, Ti-0IND, and Ti-1IND were implanted into the distal femur of mice. After two months, the mice were sacrificed and the obtained samples were analyzed by micro-CT. The images of coronal and transverse all demonstrated that newer bones were formed around the Ti-1IND group, followed by the Ti-0IND group, and the pristine Ti group displayed the worst osteointegration efficiency (Fig. 6(A)). Undecalcified sections were also prepared to conduct H and E staining and toluidine staining (Fig. 6(B) and (C), respectively). Obvious bone loss and bone volume reduction were observed around the pristine Ti bar. Bone loss was alleviated, and a denser new bone matrix around Ti-0IND and Ti-1IND implants were observed. Further quantitative analysis of micro-CT data confirmed that the three indices reflecting osteointegration efficiency (BV/TV, Tb.Th, and BIC) in the Ti-1IND group were highest, followed by the Ti-0IND group and pristine Ti group (Fig. 6(D), (E), and (F), respectively).

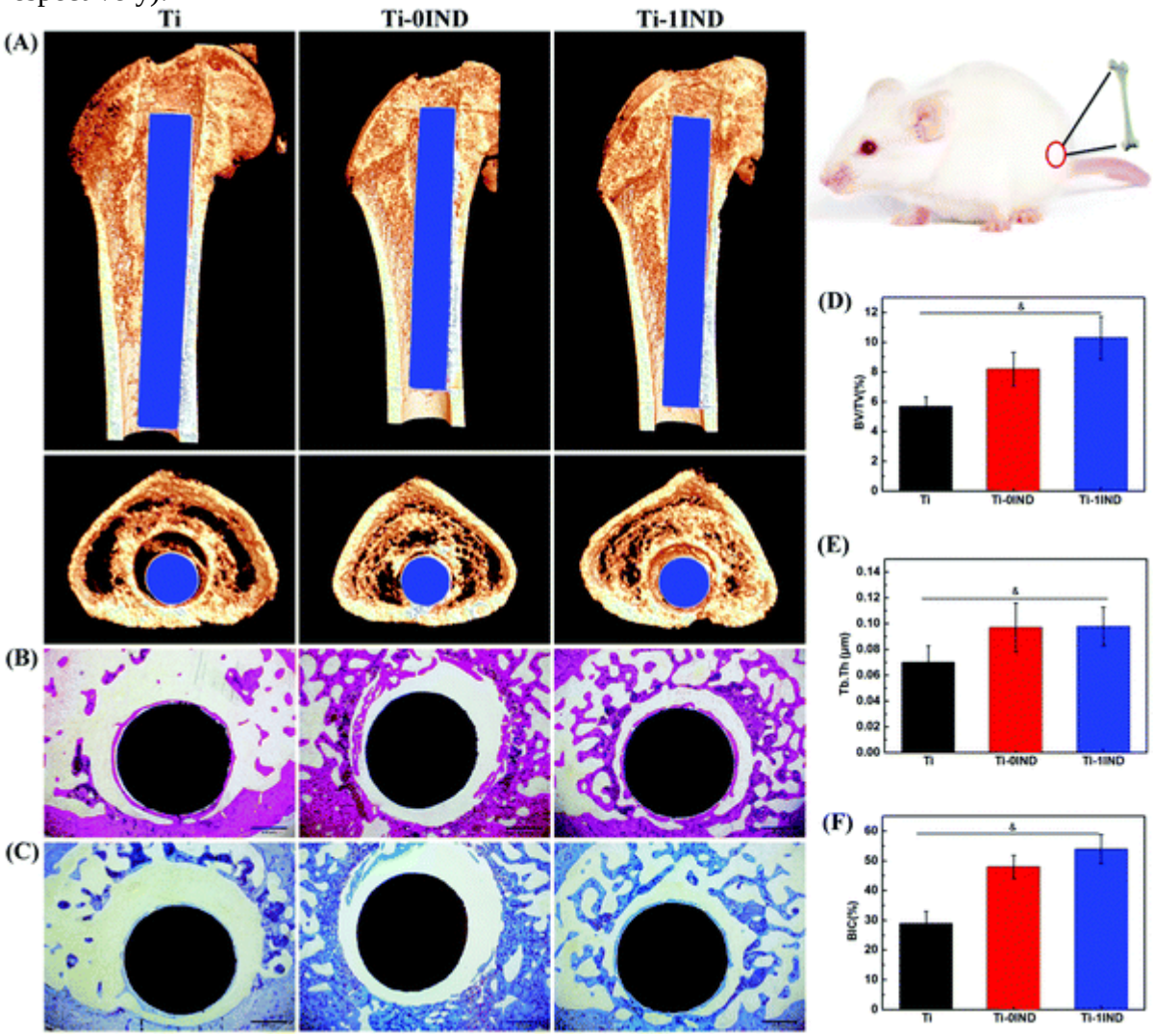

Fig. 6 (A) Representative micro-CT images from the pristine Ti, Ti-0IND, Ti-1IND groups; (B) H&E staining and (C) toluidine blue staining of the histological slice of the obtained samples, the scale bar was 500 μm; quantitative analysis of (D) BV/TV (%), (E) Tb.Th (μm), and (F) BIC (%), $n = 3$, data are mean ± s.d., $^{\&}P < 0.05$.

Generally, an acute and uncontrollable inflammatory response will impair the osteogenic differentiation. In contrast, a mild immune response induced by implants is considered beneficial for osteointegration.[26,45] The worst osteointegration efficiency of pristine Ti bar should be ascribed to the induced severe inflammatory response. As analyzed above, when macrophages were seeded onto the pristine Ti surface, a majority of macrophages were polarized to the M1 phenotype, leading to the accumulation of pro-inflammatory cytokines. In contrast, the coatings inhibited macrophage polarization from M0 to M1, leading to less accumulation of pro-inflammatory cytokines, which was demonstrated by the expression of macrophage surface marker genes, pro-inflammatory cytokine genes, as well as ELISA results. The influence of inflammatory cytokines on osteogenesis is usually dose and timing-dependent.[35]For example, IL-1β displayed a dose-dependent inhibitory effect on the osteogenic differentiation of BMSCs, *i.e.* a higher dose led to a higher inhibitory effect.[45] IL-6 was typically considered as an osteoclastogenic factor, the accumulation of which could induce bone resorption.[46] Thus, the enhanced osteointegration efficiency in the coating-modified groups may be attributed to manipulating a mild inflammatory response, in comparison with the Ti plate.

The ti-1IND group displayed better osteointegration efficiency than the Ti-0IND group. Compared with the Ti-0IND group, a higher proportion of macrophages on Ti-1IND were activated from M0 to M2 phenotype, resulting in enhanced secretion of anti-inflammatory cytokines (IL-4 and IL-10) and osteogenic-related cytokines (BMP2, TGF-β1, and VEGF). It has been widely reported that IL-4, IL-10, and TGF-β1 could induce osteoblast migration, proliferation, or secretion of bone extracellular matrix.[47] TGF-β1 and BMP2 are key signaling molecules targeting RUNx2, which can stimulate transcription of osteogenic-related genes such as OCN, COL1, and ALP.[43] Additionally, VEGF was also able to enhance osteoblast differentiation synergistically with BMP2. Thus, the osteoimmune environment manipulated by Ti-1IND was more beneficial for osteointegration.

4. Conclusions

In this study, a novel pro-drug (TA–IND) with universal adhesion and inflammatory-responsive release characteristics is firstly synthesized, then IND-loaded metal-phenolic based coating is formed by chelation with Fe^{3+}. The drug loading amounts could be tuned by controlling the grafting degree of the IND molecule or the coating thickness. The release of TA and IND motifs could be triggered in the inflammation environment, which displays inflammation-responsive self-regulated release behavior. The combination of TA and IND has synergistic effects on the immune environment, leading to the reduction of ROS, the limited expression of pro-inflammatory cytokines, and the improved secretion of anti-inflammatory and osteogenic-related cytokines. Consequently, the immune micro-environment generated by the coatings is more favorable for the osteogenic differentiation of BMSCs, thus resulting in an enhanced *in vivo* osteointegration efficiency. Therefore, the metal-phenolic-based versatile-coating strategy shows a great potential application for rendering bone implants favorable OIM function.

Conflicts of interest

There are no conflicts to declare.

Acknowledgements

This study was supported by the National Key Research and Development Program of China (Grant No. 2017YFA0104800), science and technology innovation talent program of Sichuan Province (Grant No. 20CXRC0070), National Natural Science Foundation of China (NSFC) (Grant No. 31771077), the internal funds of the Hong Kong Polytechnic University (Grant No. 1-ZE1E and G-YW4B).

References

1. G. Zhou and T. Groth , Macromol. Biosci., 2018, 18 , 1800112 —1800127
2. J. Lee , H. Byun , S. K. Madhurakkat Perikamana , S. Lee and H. Shin , Adv. Healthcare Mater., 2018, 8 , 1801106 —1801126
3. R. Zhou , D. Wei , S. Cheng , W. Feng , Q. Du , H. Yang , B. Li , Y. Wang , D. Jia and Y. Zhou , ACS Appl. Mater. Interfaces, 2014, 6 , 4797 —4811
4. S.-S. Jin , D.-Q. He , D. Luo , Y. Wang , M. Yu , B. Guan , Y. Fu , Z.-X. Li , T. Zhang , Y.-H. Zhou , C.-Y. Wang and Y. Liu , ACS Nano, 2019, 13 , 6581 —6595
5. C. Wu , Z. Chen , D. Yi , J. Chang and Y. Xiao , ACS Appl. Mater. Interfaces, 2014, 6 , 4264 —4276
6. J. L. Dziki and S. F. Badylak , Curr. Opin. Biomed. Eng., 2018, 6 , 51 —57
7. Y.-J. Huang , K.-C. Hung , H.-S. Hung and S.-H. Hsu , ACS Appl. Mater. Interfaces, 2018, 10 , 19436 —19448
8. M. L. Novak and T. J. Koh , J. Leukocyte Biol., 2013, 93 , 875 —881
9. S. Gordon Nat. Rev. Immunol., 2003, 3 , 23 —35
10. Z. Chen , A. Bachhuka , F. Wei , X. Wang , G. Liu , K. Vasilev and Y. Xiao , Nanoscale, 2017, 9 , 18129 —18152
11. H. Liang , C. Jin , L. Ma , X. Feng , X. Deng , S. Wu , X. Liu and C. Yang , ACS Appl. Mater. Interfaces, 2019, 11 , 41758 —41769
12. J. Bai , H. Wang , H. Chen , G. Ge , M. Wang , A. Gao , L. Tong , Y. Xu , H. Yang , G. Pan , P. K. Chu and D. Geng , Biomaterials, 2020, 255 , 120197
13. H. Al-Khoury , E. Espinosa-Cano , M. R. Aguilar , J. S. Román , F. Syrowatka , G. Schmidt and T. Groth , Biomacromolecules, 2019, 20 , 4015 —4025
14. Z. Chen , L. Chen , R. Liu , Y. Lin , S. Chen , S. Lu , Z. Lin , Z. Chen , C. Wu and Y. Xiao , Biomater. Sci., 2018, 6 , 1007 —1019 Search PubMed .
15. W. Zhang , F. Zhao , D. Huang , X. Fu , X. Li and X. Chen , ACS Appl. Mater. Interfaces, 2016, 8 , 30747 —30758 Search PubMed .
16. Q. Ou , K. Huang , C. Fu , C. Huang , Y. Fang , Z. Gu , J. Wu and Y. Wang , Chem. Eng. J., 2020, 382 , 123019 Search PubMed .
17. W. Zhang , X. Lu , Z. Yuan , M. Shen , Y. Song , H. Liu , J. Deng , X. Zhong and X. Zhang , Int. J. Nanomed., 2019, 14 , 977 —991 Search PubMed .
18. S. Liu , X. Zhao , J. Tang , Y. Han and Q. Lin , ACS Biomater. Sci. Eng., 2021, 7 , 1065 —1073 Search PubMed .
19. E. M. O'Brien , G. E. Risser and K. L. Spiller , Adv. Drug Delivery Rev., 2019, 149 , 85 —94 Search PubMed .

20. S. Thakur , B. Riyaz , A. Patil , A. Kaur , B. Kapoor and V. Mishra , Biomed. Pharmacother., 2018, 106 , 1011 —1023 Search PubMed .
21. J. Ran , H. Zeng , J. Cai , P. Jiang , P. Yan , L. Zheng , Y. Bai , X. Shen , B. Shi and H. Tong , Chem. Eng. J., 2018, 333 , 20 —33 Search PubMed .
22. Y. Lu , A. A. Aimetti , R. Langer and Z. Gu , Nat. Rev. Mater., 2017, 2 , 16075 Search PubMed .
23. X. Li , P. Gao , J. Tan , K. Xiong , M. F. Maitz , C. Pan , H. Wu , Y. Chen , Z. Yang and N. Huang , ACS Appl. Mater. Interfaces, 2018, 10 , 40844 —40853 Search PubMed .
24. J. Chen , J. Li , J. Zhou , Z. Lin , F. Cavalieri , E. Czuba-Wojnilowicz , Y. Hu , A. Glab , Y. Ju , J. J. Richardson and F. Caruso , ACS Nano, 2019, 13 , 11653 —11664 Search PubMed .
25. S. Chen , Y. Xie , T. Xiao , W. Zhao , J. Li and C. Zhao , Chem. Eng. J., 2018, 337 , 122 —132 Search PubMed .
26. Z. Zheng , Y. Chen , B. Guo , Y. Wang , W. Liu , J. Sun and X. Wang , Chem. Eng. J., 2020, 396 , 125241 Search PubMed .
27. A. Sivanantham , D. Pattarayan , N. Rajasekar , A. Kannan , L. Loganathan , R. Bethunaickan , S. K. Mahapatra , R. Palanichamy , K. Muthusamy and S. Rajasekaran , Inflammation Res., 2019, 68 , 1011 —1024 Search PubMed .
28. F. Hizal , I. Zhuk , S. Sukhishvili , H. J. Busscher , H. C. van der Mei and C.-H. Choi , ACS Appl. Mater. Interfaces, 2015, 7 , 20304 —20313 Search PubMed .
29. L. Hou , Y. Zheng , Y. Wang , Y. Hu , J. Shi , Q. Liu , H. Zhang and Z. Zhang , ACS Appl. Mater. Interfaces, 2018, 10 , 21927 —21938 Search PubMed .
30. A. Y. Kim , J. H. Ha and S. N. Park , Biomacromolecules, 2017, 18 , 3197 —3206 Search PubMed .
31. Y. Du , W.-Z. Qiu , Z. L. Wu , P.-F. Ren , Q. Zheng and Z.-K. Xu , Adv. Mater. Interfaces, 2016, 3 , 1600167 Search PubMed .
32. H. Ejima , J. J. Richardson and F. Caruso , Nano Today, 2017, 12 , 136 —148 Search PubMed .
33. Z. Xu , X. Wang , X. Liu , Z. Cui , X. Yang , K. W. K. Yeung , J. C. Chung , P. K. Chu and S. Wu , ACS Appl. Mater. Interfaces, 2017, 9 , 39657 —39671 Search PubMed .
34. T. S. Sileika , D. G. Barrett , R. Zhang , K. H. A. Lau and P. B. Messersmith , Angew. Chem., Int. Ed., 2013, 52 , 10766 —10770 Search PubMed .
35. Z. Chen , A. Bachhuka , S. Han , F. Wei , S. Lu , R. M. Visalakshan , K. Vasilev and Y. Xiao , ACS Nano, 2017, 11 , 4494 —4506 Search PubMed .
36. J. Kwon , J. Kim , S. Park , G. Khang , P. M. Kang and D. Lee , Biomacromolecules, 2013, 14 , 1618 —1626 Search PubMed .
37. Y. Wang , L. Li , W. Zhao , Y. Dou , H. An , H. Tao , X. Xu , Y. Jia , S. Lu , J. Zhang and H. Hu , ACS Nano, 2018, 12 , 8943 —8960 Search PubMed .
38. P. Wang , J. Liu , X. Luo , P. Xiong , S. Gao , J. Yan , Y. Li , Y. Cheng and T. Xi , J. Mater. Chem. B, 2019, 7 , 7314 —7325 Search PubMed .
39. J. Tan , Z. Deng , G. Liu , J. Hu and S. Liu , Biomaterials, 2018, 178 , 608 —619 Search PubMed .
40. Y. Arima and H. Iwata , Biomaterials, 2007, 28 , 3074 —3082 Search PubMed .
41. J. M. Sadowska , F. Wei , J. Guo , J. Guillem-Marti , M.-P. Ginebra and Y. Xiao , Biomaterials, 2018, 181 , 318 —332 Search PubMed .

42. F. Y. McWhorter , T. Wang , N. Phoebe , C. Thanh and W. F. Liu , Proc. Natl. Acad. Sci. U. S. A., 2013, 110 , 17253 —17258 Search PubMed .
43. L. Bai , Z. Du , J. Du , W. Yao , J. Zhang , Z. Weng , S. Liu , Y. Zhao , Y. Liu , X. Zhang , X. Huang , X. Yao , R. Crawford , R. Hang , D. Huang , B. Tang and Y. Xiao , Biomaterials, 2018, 162 , 154 —169 Search PubMed .
44. A. Mansour , L. Abu-Nada , H. Al-Waeli , M. A. Mezour , M.-N. Abdallah , J. M. Kinsella , J. Kort-Mascort , J. E. Henderson , J. L. Ramirez-Garcialuna , S. D. Tran , O. A. Elkashty , A. Mousa , A. A. El-Hadad , D. Taqi , F. Al-Hamad , O. Alageel , M. T. Kaartinen and F. Tamimi , Acta Biomater., 2019, 89 , 343 —358 Search PubMed .
45. D. C. Lacey , P. J. Simmons , S. E. Graves and J. A. Hamilton , Osteoarthritis Cartilage, 2009, 17 , 735 —742 Search PubMed .
46. T. J. Cho , J. A. Kim , C. Y. Chung , W. J. Yoo , L. C. Gerstenfeld , T. A. Einhorn and I. H. Choi , Calcif. Tissue Int., 2007, 80 , 192 —200 Search PubMed .
47. G. Mori , P. D'Amelio , R. Faccio and G. Brunetti , J. Immunol. Res., 2015, 2015 , 108451 Search PubMed .